Journal of Thermal Analysis and Calorimetry
https://doi.org/10.1007/s10973-020-10128-9

Thermal analysis of CuMg alloys deformed by equal channel angular pressing

Pablo Rodríguez-Calvillo[1] · Nuria Ferrer[2] · José-María Cabrera[3,4]

Received: 8 February 2020 / Accepted: 25 July 2020

Abstract
The thermal behavior of two copper alloys, with 0.2 and 0.5 mass % of Mg, was analyzed after severe plastic deformation processing by Equal Channel Angular Pressing (ECAP). Both alloys were forced to be passed through a 90º inner angle ECAP die at room temperature up to 16 passes following route Bc. The thermal stability was analyzed in terms of the recrystallization kinetics by using the Various Heating Rates method, derived from the Johnson–Mehl–Avrami–Kolmogorov equation, after analyzing the Differential Scanning Calorimetry peaks for both alloys at any pass of ECAP. The calculated recrystallization parameters included the activation energies (E (kJ mol^{-1}) $E_{CuMg02} = 42.6 \pm 19.8$ $E_{CuMg05} = 52.7 \pm 13$ kJ mol^{-1}) and the kinetic exponent n which took an average value of ≈ 1.75, irrespective of the considered alloy.

Keywords ECAP · DSC · VHR · CuMg alloy · Thermal stability

Introduction

Equal Channel Angular Pressing (ECAP) is a severe plastic deformation technique (SPD) developed in the early 70´s by Segal for producing Ultra Fine Grain (UFG) microstructures of metallic materials. As a result, this microstructural refinement promotes an increase in strength maintaining the net shape of the part. On the other hand, ECAP is the SPD process most likely to be applied at industrial scale. Nevertheless, the experimental setup (i.e., ECAP dies geometry, number of passes, velocity, lubrication, temperature and alloying elements…) defines the amount of applied deformation and/or stored energy, thus the capability for grain refinement and therefore the subsequent annealing behavior [1–5].

One potential application of the ECAP process is the fabrication of Cu alloys for power contact cables for high speed trains. When ECAP is applied to commercially pure copper, a noticeable increase in yield strength is observed while the electrical conductivity remains practically unaltered [6–10]. However, yield strength attained in pure copper after SPD is still below the value required in the above application (600–700 MPa), so some degree of alloying must be introduced. In the literature, one can find studies on the influence of certain alloying elements such as Al, Zn, Cr, Mn and Ag after ECAP [11–15], but scarce information on Mg, which is commonly added to Cu to obtain both relatively high strength and moderate to high conductivity, making Cu–Mg alloys suitable material for power contact cables, especially after ECAP processing. Traditionally, Mg additions to pure Cu range between 0.2 and 0.5 mass/%. Lower amounts do not provide enough strength and higher contents penalize electrical conductivity in excess. Maki et al. [16] studied the influence of Mg, Al, Mn and Sn as solid-solution elements in copper alloys with high strength and good electrical conductivity, reporting a great increase in the recrystallization temperature by Mg addition and after 1 h of isochronal annealing. Habibi et al. [17] processed a CuMg0.5 alloy by Equal Channel Angular Rolling (ECAR) reporting grain sizes of 0.3 µm but with a strength below 300 MPa with

✉ José-María Cabrera
jose.maria.cabrera@upc.es

1 ArcelorMittal Global R&D Gent, J.F. Kennedylaan 3, 9060 Zelzate, Belgium

2 La Farga YourCopperSolutions SA, Les Masies de Voltregà, Ctra C-17 km 73.5, 08508 Barcelona, Spain

3 Department of Materials Science and Engineering, Universitat Politècnica de Catalunya, c/ Eduard Maristany 10-14, 08019 Barcelona, Spain

4 Institute of Research in Metallurgy and Materials, Universidad Michoacana de San Nicolás de Hidalgo, Av. Francisco Múgica s/n, CU, Edificio U, 58230 Morelia, Michoacán, Mexico

Published online: 05 August 2020

81%IACS of electrical conductivity after 7 passes. Apparently, this low level of strength might be attributed to the temperature at which the ECAR was conducted that unfortunately was not reported. On the other hand, Zhu et al. [18] characterized two CuMg after four passes of ECAP followed by cold working and thermal treatment steps. They reported a tensile strength of 574.8 MPa (Cu–0.2 mass/% Mg) and 627.4 MPa (Cu–0.4 mass/% Mg) with the following electrical conductivity 81.5%IACS and 72.4%IACS, respectively. After annealing at 300 °C, their electrical conductivity values increased to around 87 and 80%IACS, respectively. Yang et al. [19] reported that after annealing at 300 °C for 2 h, Cu–0.3 Mg–0.05Ce ECAP samples still maintained excellent properties: tensile strength of 558.2 MPa, electrical conductivity of 74.7%IACS and elongation around 13.2%. Finally, present authors [20], in two Cu-Mg alloys, namely Cu–0.2 mass/% Mg and Cu–0.5 mass /% Mg, after 16 ECAP passes, found tensile strength in the order of 550 and 750 MPa with acceptable total elongation (20%). It is worth noticing that saturation in mechanical properties at increasing ECAP passes was not observed, so further hardening capacity was still present in the latter alloys. Most of all above-mentioned works refer to post-ECAP analysis, without application of any annealing treatment [16–20]. The thermal stability (i.e., the response under annealing treatments) is crucial, especially because, in service, some heating can occur in the particular application here mentioned, either by Joule effect, or by friction with the pantograph. It is well known that thermal stability of severe plastically deformed alloys tends to be lower [8, 21–23] than their undeformed counterparts, so recrystallization temperatures decrease. In certain cases, they can be very close to ambient temperature, or close enough to promote recrystallization at ambient temperature after long times (months or similar). Therefore, an analysis of the thermal stability and derivation of recrystallization kinetics equations are a must in this particular application (power contact cables) to ensure in service implementation.

On the other hand, the crystallization kinetics of metallic glasses has been successfully studied under non-isothermal conditions by the so-called Various Heating Rates (VHR) method, which is derived from the Johnson–Mehl–Avrami–Kolomogorov (JMAK) equation [24–27] after evaluation of the whole exothermic peaks at different heating and processing conditions. The recrystallization behavior of metals after ECAP processing has been, partially, characterized by Differential Scanning Calorimetry (DSC) under non-isothermal conditions. In general, only the apparent activation energy is reported for the temperature at the peak of the DSC curves [9, 10, 22, 23, 28–33] and no complete characterization of the recrystallization kinetics is reported. Cao et al. [28] gave values of apparent activation energy of 77–80 kJ mol^{-1}, for an oxygen-free high conductivity (OFHC) copper, somewhat lower than the activation energy of boundary migration in copper (104 kJ mol^{-1}). Higuera-Cobos et al. [9] calculated the apparent activation energy of an ECAPed electrolytic tough pitch (ETP copper, reporting activation energies in the range of 68–116 kJ mol^{-1}. These values were in line with the ones reported by Sakar et al. [29], who determined also an activation energy of 68 kJ mol^{-1} for ECAPed pure Cu following route Bc, and Wang et al. [30], who evaluated the effect of back pressure on the activation energies, of an ETP copper, leading to values of ~ 88.1 kJ mol^{-1} and ~ 79.2 kJ mol^{-1} for samples processed without back pressure and under a back pressure of 100 MPa, respectively. On top of these, Molodova et al. [10] have reported activation energies of isochronal annealing treatments of 65.6 kJ mol^{-1} and an Avrami exponent ≈1 virtually independent of the number of passes for pure copper. Larbi et al. [31] reported values of 123 and 127 kJ mol^{-1} for a Cu2.5Ni0.6Si alloys. Abib et al. [32] determined an activation enthalpy value for recrystallization of 117.12 kJ mol^{-1} after 16 ECAP passes in $Cu-1Cr-0.1Zr$. More recently, Fellah et al. [33] calculated the activation energy of the recrystallization of pure Cu reporting average values between 92.55 and 52.10 kJ mol^{-1} observing a decrease with the increase in reduction during cold-wire drawing, i.e., with the total amount of strain impaired.

Therefore, the present work is focused on the thermal analysis of the annealing behavior of two commercially CuMg alloys, after SPD processing by means of ECAP technology, from the interpretation of the so-called VHR method.

Experimental

Commercially available copper with Mg mass/% of 0.22 and 0.52 according to chemical composition shown in Table 1, denoted as CuMg0.2 and CuMg0.5, respectively, and supplied in as-cast state, were processed via ECAP. The ECAP setup was specifically designed to apply a total true strain of 1 per pass. Full details of die geometry, experimental processing conditions, mechanical and microstructure characterization can be found elsewhere [20]. The latter study was conducted in a 90º ECAP die after 1, 2, 4, 6 and 8

Table 1 Chemical composition (mass/ppm), with Cu to balance

	Ag	Mg	Sn	O	Other elements
CuMg0.2	12	2229	0	3	32
CuMg0.5	8	5188	1	10	20

passes. Traditionally, and depending on the initial grain size, a microstructural steady state is reached after 4–6 passes. In order to be sure that such steady state was reached, an additional ECAP sample with 16 passes was performed. It was observed (Figs. 5, 6 and 9 in reference [20]) that such microstructural saturation was basically reached after 8 passes in the CuMg0.2 alloy while in the CuMg0.5 such saturation was not yet attained after 16 passes. However, the reduction in grain size from 8 to 16 passes in this latter alloy, although significant, was relatively minor, so it was assumed that the CuM0.5 alloy after 16 passes was almost in the steady sate. In consequence, no extra samples were pressed between 8 and 16 passes.

The recrystallization kinetics of the materials were determined by differential scanning calorimetry, DSC, using as LABYS EVO SETARAM calorimeter under constant heating rate of 10, 20 and 40 ºC min^{-1} in an N_2 atmosphere, with temperature varying from room temperature to 600 ºC, by the VHR method. Samples ranging 40–50 g were used for this purpose. The range of heating rates tested is expected to be able to clearly detect its effect on the recrystallization kinetics. They are also in the range of similar studies reported in the literature [34–37]. Because the aim was solely the derivation of the recrystallization kinetics, no microstructural analysis was necessary to be carried out.

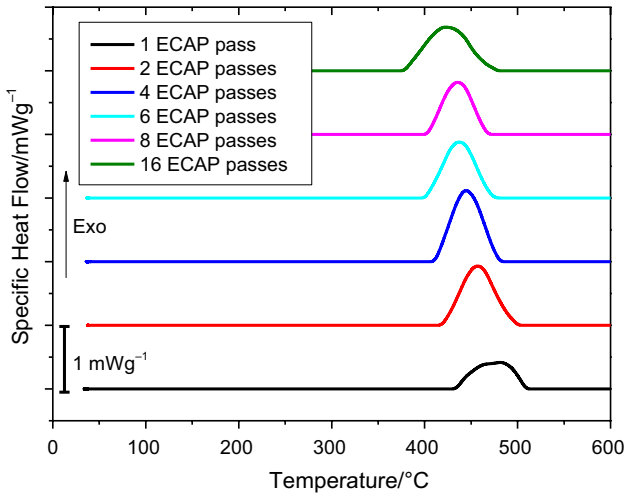

Fig. 1 DSC curves of CuMg0.5 at 10 ºC min^{-1} for different number of ECAP passes

Results and discussion

Thermal behavior and recrystallization

Figure 1 shows, as an illustrative example, the DSC curves of CuMg0.5 with different levels of deformation, i.e., ECAP passes, at a heating rate of 10 ºC min^{-1}. An exothermic peak is apparent which shifts toward lower temperatures at increasing strain. This was also observed in all heating rates (10, 20 and 40 ºC min^{-1}) and in both alloys. This exothermic peak is associated to the release of energy during the recrystallization process. On the other hand, the onset temperature for recrystallization T_o and the temperature associated with the maximum heat flow T_p are illustrated in Fig. 2 for both alloys and all heating rates. It is evident that the diminution in both temperatures is stronger at low number of ECAP passes, while a saturation is noticed at larger number of passes. As well the lower the heating rate, the lower the recrystallization temperature. This also applies to the Mg content, where lower alloying amount promotes lower recrystallization temperatures.

The recrystallization fraction of metallic materials has been extensively investigated using the Johnson–Mehl–Avrami–Kolmogorov (JMAK) model described below [10, 24–27]

$$X(t) = \frac{S_j}{S} = 1 - \exp\left[-(Kt)^n\right] \quad (1)$$

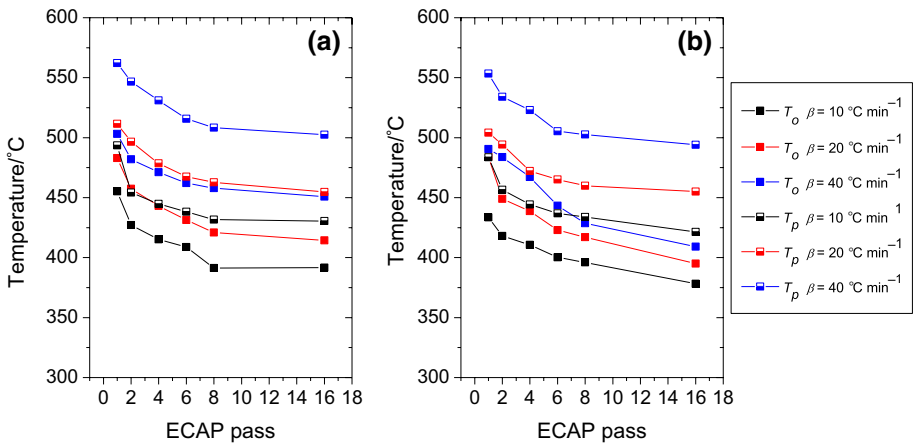

Fig. 2 Variation of both onset (T_o) and peak (T_p) temperatures for alloys **a** Cu0.2 Mg and **b** Cu0.5 Mg as a function of the ECAP pass

where $X(t)$ is the volume fraction recrystallized in a time t, S is the total surface of the exothermic peak, Sj the partial surface at any temperature, n is the Avrami exponent which reflects the nucleation and growth mechanism, and K is an effective overall reaction rate constant for nucleation and growth during recrystallization, often written by an Arrhenius temperature dependence as:

$$K(T) = K_o \exp\left[-\frac{E}{RT}\right] \tag{2}$$

being E the apparent activation energy for the recrystallization process (J mol^{-1}), K_o (s^{-1}) a frequency factor, T the absolute temperature, and R is the gas constant equal to 8.314 kJ mol^{-1} K^{-1}).

Activation energy

Several authors have calculated the apparent activation energy of pure Cu under non-isothermal conditions by the Kissinger (Eq. 3), Ozawa (Eq. 4) and Bessel (Eq. 9) methods, given by the following expressions [8, 9, 14, 33, 38, 39]:

$$\mathrm{Ln}\left(\frac{\beta}{T_p^2}\right) = -\frac{E}{RT_p} + \text{Constant} \tag{3}$$

$$\mathrm{Ln}(\beta) = -\frac{E}{RT_p} + \text{Constant} \tag{4}$$

$$\mathrm{Ln}\left(\frac{\beta}{T_p}\right) = -\frac{E}{RT_p} + \text{Constant} \tag{5}$$

where β is the heating rate, R is the gas constant and T_p is the temperature corresponding to the maximum heat flow. In most cases, this temperature is also associated with the 50% of volume transformation, i.e., $X = 0.5$. On the other hand, the VHR method allows the determination of the apparent activation energy considering equal fractions of recrystallization using the following expressions [40]:

$$\mathrm{Ln}(t_i) = \frac{E}{RT_i} + \mathrm{Ln}\theta_i \tag{6}$$

$$\theta_i = \frac{\left[-\mathrm{Ln}\left(1 - X_i\right)\right]^{1/n}}{K_0} \tag{7}$$

where t_i is the time to reach a given i temperature counting from T_o, thus equals to $(T_i - T_o)/\beta$. This Eq. (6) is similar to the Augis and Bennett's expression, which is an extension of the Kissinger method and believed to be more accurate [39, 40]. Plot of Fig. 3a shows the dependence of ln(t) versus T^{-1} of data obtained for a given recrystallization fraction, X, from 0.2 to 0.8 for the CuMg0.5 alloy after 1 ECAP pass. In this work, all the evaluation of recrystallization takes into account recrystallization fraction from 0.2 to 0.8. The calculated apparent activation energies as a function of recrystallization fraction and ECAP pass are presented in Fig. 3b showing that in most passes, slight variation of the apparent activation energies can be noticed. For instance, at 1 and 2 ECAP passes, a slight diminution is noticed, while at 4 and 6 passes, a slight increase is evident. Stronger variations are observed at 8 and 16 passes specially at low recrystallization fractions. However, out of these two latter observation, differences are in the range of 5 kJ mol^{-1}, and in consequence, they will be assumed as part of the experimental error.

The Kissinger, Ozawa and Bessel methods consider the influence of heating rate in the determination of the activation energy and lead to systematically different values in comparison with the VHR method, as shown in Fig. 4 where only the fraction of $X = 0.5$ (or values at T_p) were considered for the calculation of the activation energies leading to $E_{\mathrm{Ozawa}} > E_{\mathrm{Bessel}} > E_{\mathrm{Kissinger}} > E_{\mathrm{VHR}}$. These differences

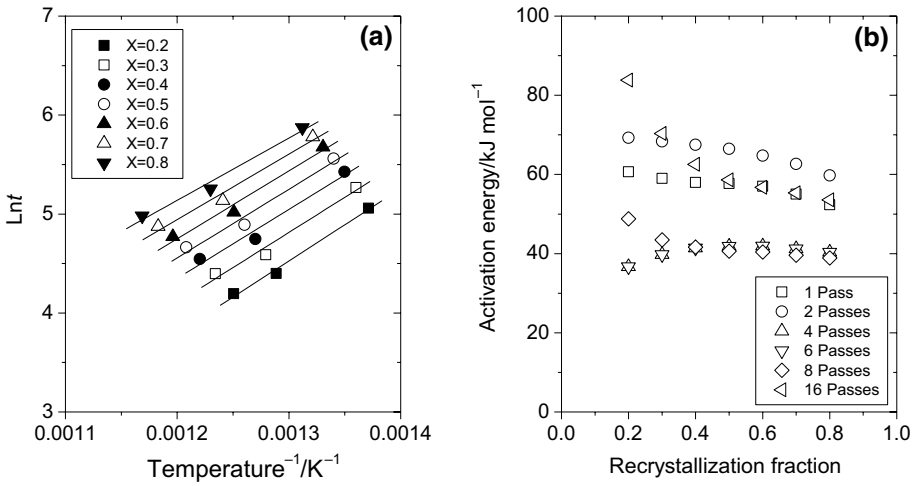

Fig. 3 **a** Representation of the relation between ln(t) versus T^{-1} in the alloy CuMg0.5 with 1 pass of ECAP, **b** Apparent activation energies E calculated with the VHR method as function of amount of recrystallization X and ECAP passes for the same alloy

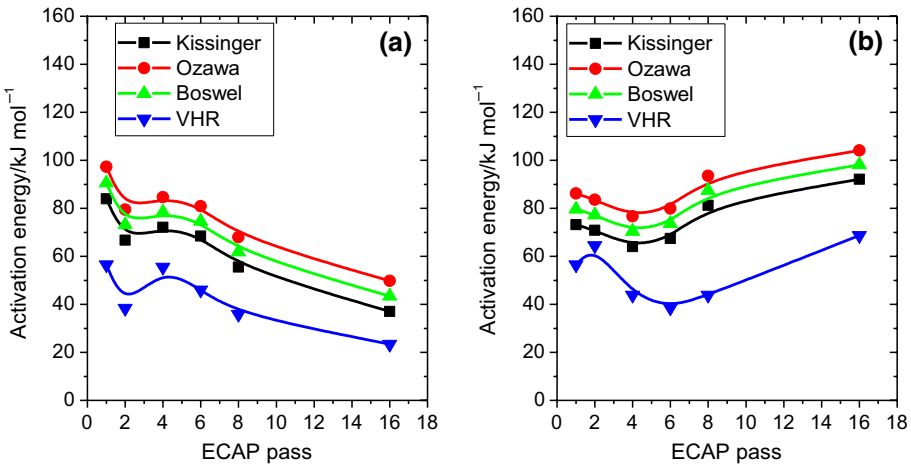

Fig. 4 Evolution of the apparent activation energy E for recrystallization calculated by the Kissinger, Ozawa, Bessel and VHR methods considering the peak temperature for alloys **a** Cu0.2 Mg and **b** Cu0.5 Mg

are attributed to the fact that the VHR method takes into consideration the subtraction of the time to reach the onset temperature [39, 40]. It is clear that all four methods predict the same tendency. The reason for the ups and downs in Fig. 4 as well than the variations commented in Fig. 3 can be explained in terms of the nature of the grain boundaries generated after each ECAP pass. It was shown elsewhere (Figs. 5a and 6 of reference [20]) that High and Low Angle Grain Boundaries (HAGB, LAGB) of present alloys follow a smooth dependence on the number of ECAP passes, while special boundaries, such as the Coincidence Site Lattice (CSL) (Σ3, Σ5, Σ7, Σ9, Σ11 and Σ27) displayed a dependence on the ECAP passes similar to the oscillation of the current activation energies. No need to mention that CSL are more stable than ordinary HAGB and LAGB, and this can clearly affect the activation energy for recrystallization.

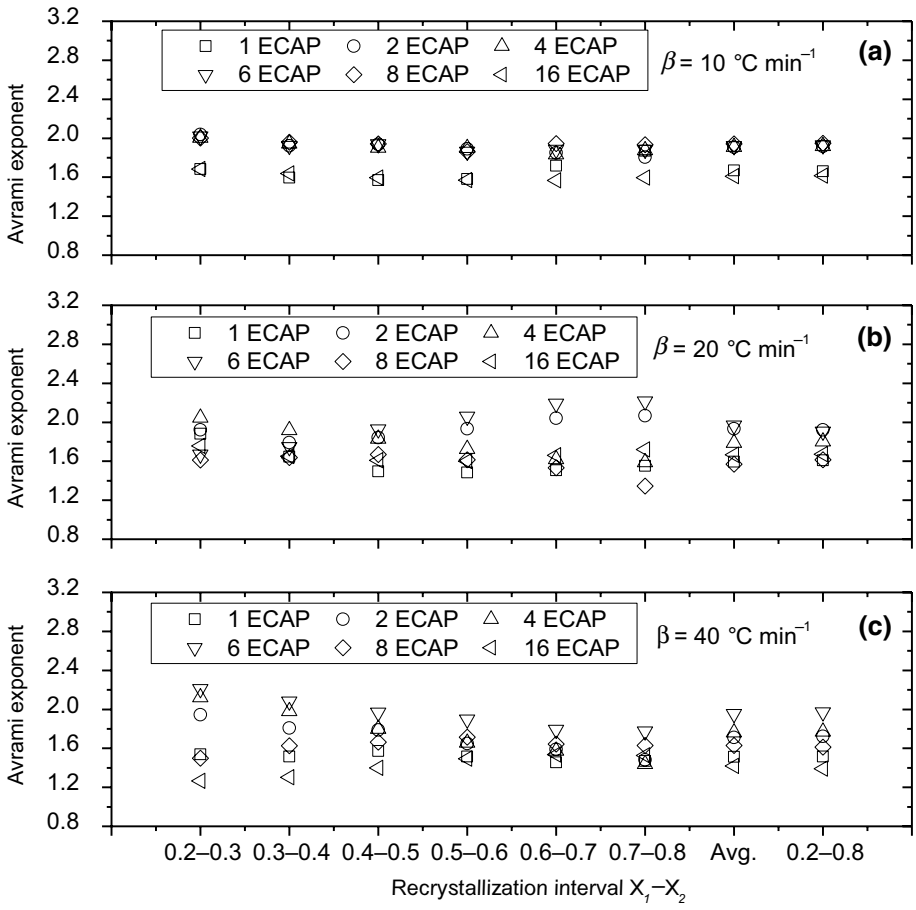

Fig. 5 Representation of the Avrami exponent n as a function of the recrystallization fraction intervals used for calculation by Eq. (8), ECAP pass and heating rate β for the CuMg0.5 alloy

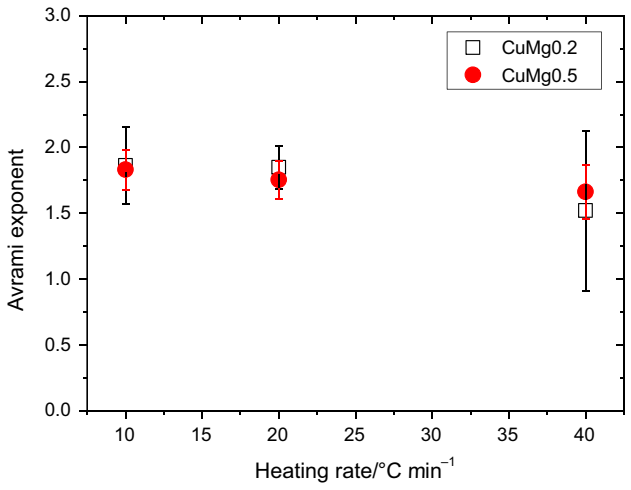

Fig. 6 Evolution of the average Avrami exponent n as a function of the heating rate β for both CuMg alloys

In any case, the total frequency of all CSL's represents less than 10% of the grain boundaries at any deformation condition and/or CuMg alloy. Accordingly, it will be here assumed that the activation energy can be considered constant irrespective of the ECAP pass. For that reason, an average value will be considered. The goodness of this assumption will be shown later by the good fitting between experimental and predicted data. The average values of activation energy for recrystallization fraction of $X=0.5$, calculated using Eq. (6), are $E_{CuMg02}=42.9\pm17.5$ kJ mol^{-1} and $E_{CuMg05}=52.2\pm11.2$ kJ mol^{-1}.

As shown in Table 2, two other values of recrystallized volume fraction, namely $X_1=0.2$ and $X_2=0.8$, were also selected to obtain E by the VHR method. Subsequently, the calculated values of $E_{CuMg02}=42.6\pm19.8$ kJ mol^{-1} and $E_{CuMg05}=52.7\pm13.9$ kJ mol^{-1} will be used for the next determinations of n and K_o in Eqs. (1) and (2).

On the other hand, the E values, calculated using the T_p or the VHR method and the values of Table 3, are quite similar although the ones of the VHR present a slightly larger standard deviation. Furthermore, it is quite surprising that present E values are far below to the ones reported for pure copper for lattice diffusion, boundary diffusion and core diffusion (197, 104 and 117 kJ mol^{-1}, respectively [37]), and also lower than the activation energies for recrystallization of Cu–2.5Ni–0.6Si (123–127 kJ mol^{-1}) found by Larbi et al. [31], in the lower limit of the values reported by Higuera-Cobos et al. (between 62.7 and 116 kJ mol^{-1}) [8, 9], but similar to those reported by Molodova et al. and Benchabane

Table 2 Temperatures T_1 and T_2/ºC and times t_1 and t_2/s obtained at volume fractions of $X_1=0.2$ and $X_2=0.8$ from the recrystallization fraction curves of CuMg alloys at 10, 20 and 40 ºC min^{-1}

ECAP pass	Alloys	Volume fraction							
		$X_1=0.2$				$X_2=0.8$			
		CuMg0.2		CuMg0.5		CuMg0.2		CuMg0.5	
	Heating rate/ ºC min^{-1}	t_1	T_1	t_1	T_1	t_2	T_2	t_2	T_2
1	10	140.8	478.7	157.6	456.2	302.0	505.5	355.6	489.1
	20	67.6	505.9	81.4	502.9	172.6	541.4	191.4	540.0
	40	53.8	541.7	66.4	526.6	148.4	608.2	145.8	582.5
2	10	96.8	443.3	171.6	443.0	233.6	466.1	342.8	471.5
	20	76.6	483.7	84.0	473.5	160.2	512.1	170.4	502.9
	40	56.0	522.1	55.8	518.0	106.0	557.6	116.4	560.9
4	10	105.2	432.8	150.4	432.1	243.2	455.9	305.6	458.2
	20	70.0	467.2	79.8	461.6	153.6	495.7	169.4	492.1
	40	46.4	504.6	66.8	509.6	91.8	536.9	130.8	555.0
6	10	106.8	426.6	161.2	423.6	242.0	449.2	321.2	450.3
	20	66.8	454.5	97.0	440.5	148.0	482.1	188.4	471.8
	40	51.6	499.4	83.2	491.8	101.4	534.8	144.8	535.7
8	10	161.6	418.5	142.4	422.8	299.6	441.7	288.4	447.3
	20	84.8	450.4	91.6	441.3	177.2	481.9	204.8	479.9
	40	53.4	496.7	77.8	473.4	199.0	600.1	151.2	526.2
16	10	151.6	417.1	190.0	406.5	332.0	447.3	404.4	442.4
	20	76.8	440.9	88.0	435.1	173.6	474.0	189.0	469.7
	40	66.4	498.8	87.2	447.1	216.4	605	176	511

Table 3 Recrystallization kinetic parameters E, n and K_o by the VHR method of the present CuMg alloys processed by ECAP

	CuMg0.2		CuMg0.5	
	Avg	SD	Avg	SD
Frequency factor, K_o/s^{-1}				
N° ECAP pass				
1	3.62	0.71	16.41	1.30
2	5.45	0.71	22.19	3.47
4	6.59	0.92	24.95	4.33
6	6.93	0.93	26.45	5.57
8	5.16	1.49	28.24	3.12
16	5.18	1.99	29.37	5.99
Avrami exponent, n				
Heating rate, K/min				
10	1.86	0.29	1.83	0.15
20	1.85	0.16	1.75	0.14
40	1.52	0.61	1.66	0.20
Activation energy, E/kJ mol^{-1}				
	42.63	19.84	52.66	13.93

et al., (57.89 and 58.63 kJ mol^{-1}) respectively, for pure Cu [10, 38]. Additionally, these values are somewhat above the one for static recovery, 48 kJ mol^{-1} [41, 42], which is also the energy for dislocation annihilation by glide or cross-slip. The latter value, as already reported by Hutchinson et al. [43], it is not clear why it should indicate the recover kinetics since grain boundary diffusion cannot be the operative mechanism in this case. Fellah et al. [33] have observed similar behavior with the calculation method and for the range of strain below 4, the activation energy was systematically reduced. The differences in the present reported activation energies might be related, on one hand, to the influence of the Mg as alloying element in reducing the stacking fault energy of Cu [13, 44]. On the other hand, these differences have been already discussed by Butrymowicz et al. [45], showing that literature presents activation energies differing by a factor of two or more (from 68 to 252 kJ mol^{-1}), and they might be attributed to oxygen and hydrogen content and crystallography orientation.

Avrami exponent

Table 2 shows the values used to calculate the apparent activation energy for the different materials and ECAP passes. The average apparent activation energy values, considering $X_1 = 0.2$ and $X_2 = 0.8$ given in Table 3, were considered for the calculation of the Avrami exponent, based on Eqs. (1) and (2), using the non-isothermal method [30, 39] and the following equation [40]:

$$n = \frac{\mathrm{Ln}\left[\frac{\mathrm{Ln}(1-X_1)}{\mathrm{Ln}(1-X_2)}\right]}{\left(\frac{E(T_1-T_2)}{RT_1T_2}\right) - \mathrm{Ln}\left(\frac{T_2}{T_1}\right)} \tag{8}$$

The n-values were calculated taking consecutives fractions of recrystallization and $X_1 = 0.2$ and $X_2 = 0.8$. Figure 5 shows the evolution of CuMg0.5 n-values with the interval fraction considered for the calculation and as a function of the ECAP pass for different heating rates. It is possible to observe a slight variation of n-values with the amount of deformation and recrystallization fraction considered, but when the average and determined values of Table 2 are compared, the differences are negligible.

Figure 6 represents the average n-values with their standard deviation for both CuMg alloys when Eq. (8) is solved using the values of Table 2. It is possible to observe that the faster the heating rates the larger the standard deviation and that remains relatively constant with respect to heating rate and/or ECAP pass. This effect has been already observed by Molodova et al. [10] for pure Cu reporting an average value of approximately 1. On the other hand, Benchabane et al. [38] obtained an Avrami exponent of 1.4 for pure cold rolled Cu. The calculated average n-values on this work together with their standard deviation are listed in Table 3, for different heating rates and alloys, which show a slight diminution with increasing heating rate and Mg content. The n-values are just below 2, being the average value for both CuMg alloys equal to 1.74, which imply that the restoration mechanism for both CuMg alloys is meanly related to volume nucleation and one-dimensional growth [46].

Frequency factor

The obtained values of E and n, Table 3, were used to calculate the frequency factor K_o as follows [40]:

$$K_o = \frac{\left[-\mathrm{Ln}\left(1 - X_i\right)\right]^{\frac{1}{n}}}{t_i \exp\left[\frac{-E}{RT_i}\right]} \tag{9}$$

With the calculation of the frequency factor, the recrystallization process of the CuMg can now be fully described and understood. Figure 7 shows the calculated frequency factors

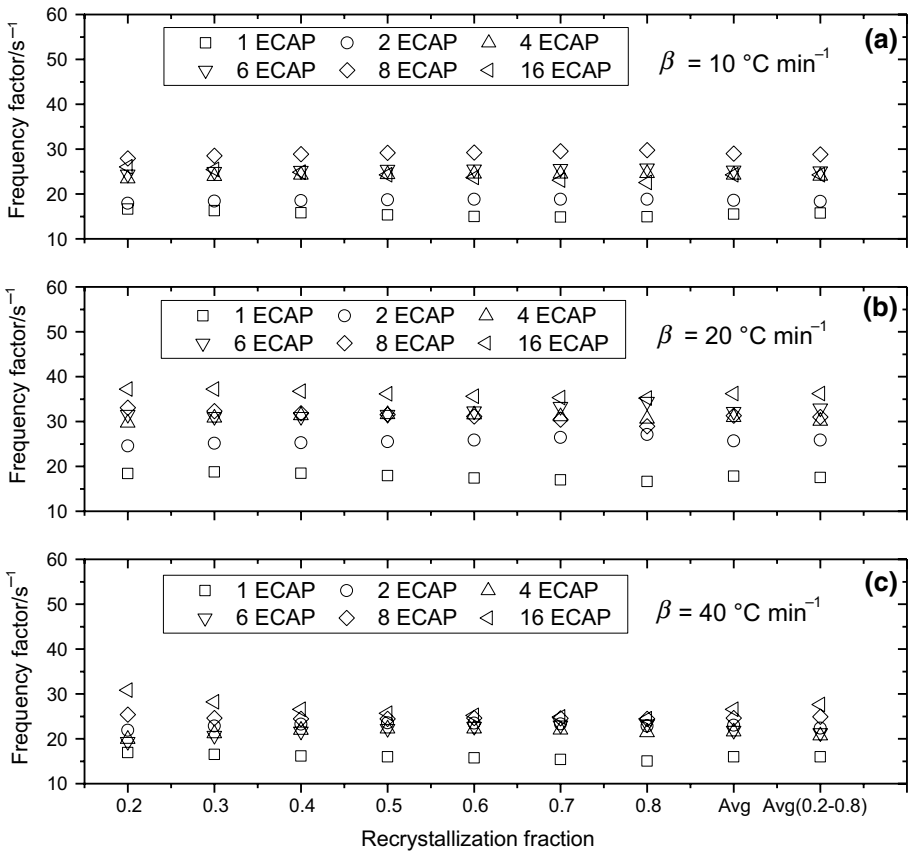

Fig. 7 Evolution of the frequency factor K_o with the recrystallization fraction X as a function of number of ECAP pass and heating rate β for the CuMg0.2

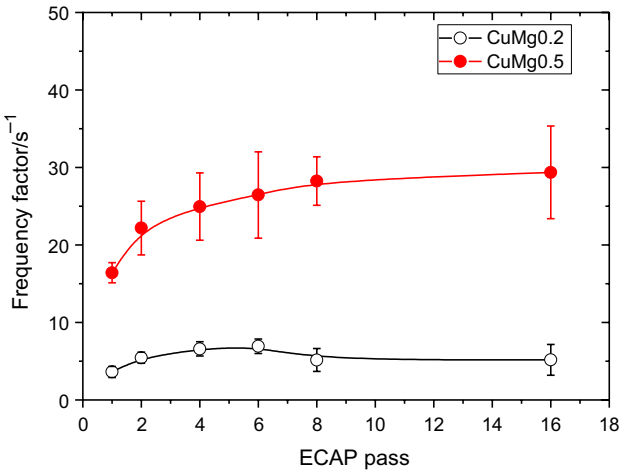

Fig. 8 Evolution of the frequency factor K_o with number of ECAP passes and heating rate β for alloys **a** CuMg0.2 and **b** CuMg0.5

K_o at different recrystallization fractions as a function of ECAP passes and heating rates, for the CuMg0.5 alloys. As shown for the Avrami exponent n, the frequency factor K_o (see Fig. 7) is quite independent on the recrystallization fraction and/or heating rate, but on the contrary, the larger the ECAP pass the larger the frequency factor K_o. This evolution is better illustrated in Fig. 8, where the average frequency factor K_o, calculated from data of Tables 2 and 3, together with their standard deviation is represented for both CuMg alloys. It is also shown in Fig. 8 that the frequency factor increases with deformation up to a maximum. In the case of the CuMg0.2 that maximum is reached at the 6th ECAP pass and then the K_o value drops to a kind of steady state. This maximum is less evident for the CuMg0.5 alloys due to the larger experimental deviation, especially in the data corresponding at 6 and 16 ECAP passes.

All the calculated parameters, listed in Table 3, were used to solve Eq. (1) at different ECAP passes, heating rates and Mg content. The comparison of the experimental and the calculated recrystallization fractions as a function of temperature, shown in Fig. 9, displays a good agreement, making the present calculation highly reliable.

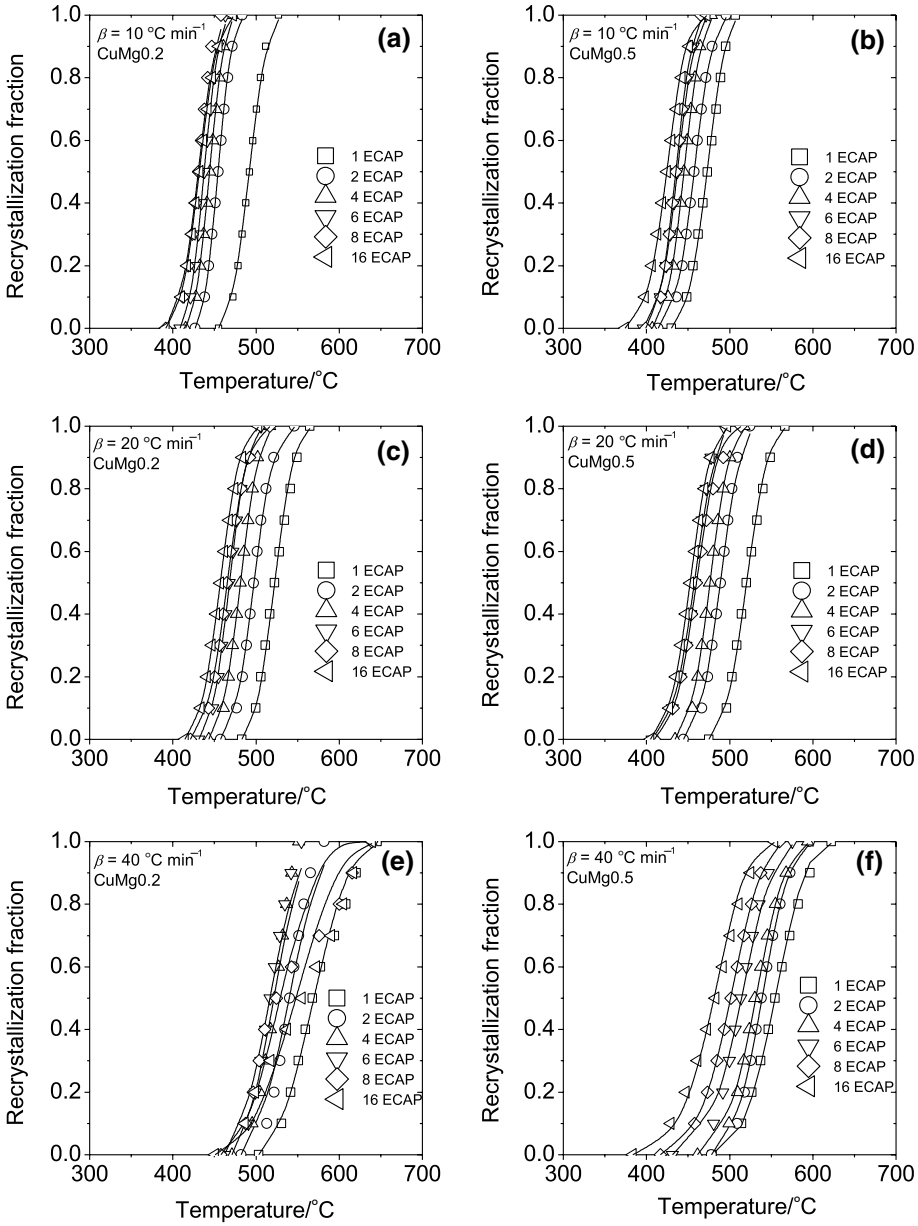

Fig. 9 Recrystallization kinetics for both CuMg alloys calculated at different heating rates. The open symbols correspond to experimental data extracted from DSC curves at different ECAP passes and the solid lines to the calculated ones using parameters of Table 3

Conclusions

The thermal behavior of two CuMg alloys severely plastic deformed by ECAP was characterized by DSC and the so-called VHR method allows withdrawing the following conclusions:

- The calculation of activation energies with other non-isochronal methods results in different apparent values, which can be ranked as $E_{Ozawa} > E_{Bessel} > E_{Kissinger} > E_{VHR}$.
- Average apparent activation energies, calculated using the VHR method, were 42.6 and 52.70 kJ mol^{-1} for CuMg0.2 and CuMg0.5 alloys, respectively, and close to the static recovery one
- The Avrami exponents showed little influence on the heating rate, number of ECAP pass or Mg content, being the average value for both alloys 1.74, which indicated that the restoration is meanly related to volume nucleation and one-dimensional growth.
- The frequency factors K_o presented some dependency on the number of ECAP pass and Mg content

Acknowledgements The authors are grateful the Generalitat de Catalunya and the European Commission for the support provided for

this research, through ACC1Ó and FEDER resources, respectively, as part of the NUCLIS (Cooperative Technological Innovation Nuclei) Programme. JMC is also grateful to CONACYT (Mexico) for partial funding his sabbatical leave in UMSNH.

Compliance with ethical standards

Conflict of interest The authors declare that they have no conflict of interest.

References

1. Segal VM. Materials processing by simple shear. Mater Sci Eng A. 1995;197:157–64.
2. Valiev RZ, Langdon TG. Principles of equal-channel angular pressing as a processing tool for grain refinement. Prog Mater Sci. 2006;51:881–981.
3. Segal VM. Mechanics of continuous equal-channel angular extrusion. J Mater Process Technol. 2010;210:542–9.
4. Azushima A, Kopp R, Korhonen A, Yang DY, Micari F, Lahoti GD, Groche P, Yanagimoto J, Tsuji N, Rosochowski A, Yanagida A. Severe plastic deformation (SPD) processes for metals. CIRP Ann Manuf Technol. 2008;57:716–35.
5. Estrin Y, Vinograd A. Extreme grain refinement by severe plastic deformation: a wealth of challenging science. Acta Mater. 2013;61:782–817.
6. Lugo N, Llorca N, Cabrera JM, Horita Z. Microstructures and mechanical properties of pure copper deformed severely by equal-channel angular pressing and high pressure torsion. Mater Sci Eng A. 2008;477:366–71.
7. Kvackaj T, Kovacova A, Kvackaj M, Kocisko R, Litynska-Dobrzynska L, Stoyka V, Mihailikova M. TEM studies of structure in OFHC copper processed by equal channel angular rolling. Micron. 2012;43:720–4.
8. Higuera-Cobos OF, Cabrera JM. Mechanical, microstructural and electrical evolution of commercially pure copper processed by equal channel angular extrusion. Mater Sci Eng A. 2013;571:103–14.
9. Higuera-Cobos OF, Calvillo PR, Cabrera JM. Thermal stability and microstructural behavior of ECAP processed copper. AIP Conf Proc. 2011;1353:553–8.
10. Molodova X, Gottstein G, Winning M, Hellmig RJ. Thermal stability of ECAP processed pure copper. Mater Sci Eng A. 2007;460–461:204–13.
11. Qu S, An XH, Yang HJ, Huang CX, Yang G, Zang QS, Wang ZG, Wu SD, Zhang ZF. Microstructural evolution and mechanical properties of Cu–Al alloys subjected to equal channel angular pressing. Acta Mater. 2009;57:1586–601.
12. Ko YG, Namgung S, Lee BU, Shin DH. Mechanical and electrical responses of nanostructured Cu–3 wt%Ag alloy fabricated by ECAP and cold rolling. J Alloys Comp. 2010;504S:S448–S45151.
13. Zhang ZJ, Duan QQ, An XH, Wu SD, Yang G, Zhang ZF. Microstructure and mechanical properties of Cu and Cu–Zn alloys produced by equal channel angular pressing. Mater Sci Eng A. 2011;528:4259–67.
14. Wei KX, Wei W, Wang F, Du QB, Alexandrov V, Hu J. Microstructure, mechanical properties and electrical conductivity of industrial Cu–05%Cr alloy processed by severe plastic deformation. Mater Sci Eng A. 2011;528:1478–84.
15. Xu CZ, Wang QJ, Zheng MS, Zhu JW, Li JD, Huang MQ, Jia QM, Du ZZ. Microstructure and properties of ultra-fine grain Cu–Cr alloy prepared by equal-channel angular pressing. Mater Sci Eng A. 2007;459:303–8.
16. Maki K, Ito Y, Matsunaga H, Mori H. Solid-solution copper alloys with high strength and high electrical conductivity. Scripta Mater. 2012;68:777–80.
17. Habibi A, Ketabchi M, Eskandarzadeh M. Nano-grained pure copper with high-strength and high-conductivity produced by equal channel angular rolling process. J Mater Process Technol. 2011;211:1085–90.
18. Zhu C, Ma A, Jiang J, Li X, Song D, Yang D, Yuan Y, Chen J. Effect of ECAP combined cold working on mechanical properties and electrical conductivity of conform-produced Cu–Mg alloys. J Alloys Comp. 2014;582:135–40.
19. Yang G, Li Z, Yuan Y, Lei A. Microstructure, mechanical properties and electrical conductivity of Cu–0.3Mg–0.05Ce alloy processed by equal channel angular pressing and subsequent annealing. J Alloys Comp. 2015;640:347–54.
20. Rodríguez-Calvillo P, Ferrer N, Cabrera JM. Analysis of microstructure and strengthening in CuMg alloys deformed by equal channel angular pressing. J Alloys Comp. 2015;626:340–8.
21. Gleiter H. Nanostructured materials: basic concepts and microstructure. Acta Mater. 2000;48:1–29.
22. Lugo N, Llorca N, Suñol JJ, Cabrera JM. Thermal stability of ultrafine grains size of pure copper obtained by equal-channel angular pressing. J Mater Sci. 2010;45:2264–73.
23. Muñoz JA, Higuera OF, Hernández-Expósito A, Boulaajaj A, Bolmaro RE, Dumitru FD, Rodriguez-Calvillo P, Moreira Jorge A, Cabrera JM. Thermal stability of ARMCO iron processed by ECAP. Int J Adv Manuf Technol. 2018;98:2917–32.
24. Kolmogorov AN. On the statistical theory of metal crystallization. Izv Akad Nauk SSSR Ser Mat. 1937;3:355–60.
25. Johnson WA, Mehl RF. Reaction kinetics in processes of nucleation and growth. Trans AIME. 1939;1352:416–42.
26. Avrami M. Kinetics of phase change. I. General theory. J Chem Phys. 1939;7:1103–12.
27. Avrami M. Kinetics of phase change. II. Transformation-time relations for random distribution of nuclei. J Chem Phys. 1940;8:212–24.
28. Cao WQ, Gu CF, Pereloma EV, Davies CHJ. Stored energy, vacancies and thermal stability of ultra-fine grained copper. Mater Sci Eng A. 2008;492:74–9.
29. Sarkar A, Suwas S, Goran D, Funderberger JJ, Toth LS, Grosdidier T. Equal channel angular pressing processing routes and associated structure modification: a differential scanning calorimetry and X-ray line profile analysis. Powder Diffr. 2012;27:194–9.
30. Wang Y, Lapokov R, Wang JT, Estrin Y. Effect of back pressure on the thermal stability of severely deformed copper. IOP Conf Ser Mater Sci Eng. 2014;63:012168.
31. Larbi FH, Abib K, Khereddine Y, Alili B, Kawasaki M, Bradai D, Langdon TG (2013) DSC analysis of an ECAP-deformed Cu–Ni–Si Alloy. Metal, Brno, Czech Republic, EU
32. Abib K, Hadj Larbi F, Rabhi L, Alili B, Bradai D. DSC analysis of commercial Cu–Cr–Zr alloy processed by equal channel angular pressing. Trans Nonferrous Met Soc China. 2015;25:838–43.
33. Fellah L, Diha A, Boumerzoug Z. Microstructural study and recrystallization kinetics of deformed commercial copper wires. Acta Metall Slovaca. 2018;24:32–42.
34. Pinto RDA, Ferreira LDR, Silva RAG. Effects of Co and Zr additions on the thermal behavior of the Cu81Al19 alloy. J Therm Anal Calorim. 2019;138:3525–33.
35. Souza JS, Modesto DA, Silva RAG. Thermal behavior of the as-cast Cu–11Al–10Mn alloy with Sn and Gd additions. J Therm Anal Calorim. 2019;138:3517–24.
36. Hachouf M, Hamana D. Effect of Bi addition on precipitation and dissolution in Cu–9at%In and Cu–5at% Sb alloys. J Therm Anal Calorim. 2020;139:75–877.

37. Wang Z, Wei R, Ouyang D, Wang J. Investigation on thermal stability and flame spread behavior of new and aged fine electrical wires. J Therm Anal Calorim. 2020;140:157–65.
38. Benchabane G, Boumerzoug Z, Gloriant T, Thibon I. Microstructural characterization and recrystallization kinetics of cold rolled copper. Physica B: Cond Matter. 2011;406:1973–6.
39. Pratap A, Patel AT. Crystallization kinetics of metallic glasses. Advances in crystallization processes. In: Y. Mastai (Ed.), http://www.intechopen.com/books/advances-in-crystallization-processes (2012)
40. Abd El-Raheem MM, Ali HM. Crystallization kinetics determination of Pb15Ge27Se58 chalcogenide glass by using the various heating rates (VHR) method. J Non-Crystalline Solids. 2010;356:77–82.
41. Frost HJ, Ashby MF. Deformation-Mechanism maps. Oxford: Pergamon; 1982.
42. Kuo CM, Lin CS. Static recovery activation energy of pure copper at room temperature. Scripta Mater. 2007;57:667–70.
43. Hutchinson WB, Ray RK. Influence of phosphorus additions on annealing behaviour of cold-worked copper. Metal Sci. 1979;13:125–30.
44. Dieter GE. Mechanical Metallurgy. London: McGraw-Hill Book Company; 1988.
45. Butrymowicz DB, Manning JR, Read ME. Diffusion in copper and copper alloys. J Phys Chem Ref Data. 1977;6:1–50.
46. Christian JW. The theory of transformation in metals and alloys. New York: Pergamon Press; 2002.